A coupled closed-form/Doubly Asymptotic Approximation approach for the response of orthotropic plates subjected to an underwater explosion

Ye Pyae Sone Oo, Hervé Le Sourne, Olivier Dorival

Ships and Offshore Structures

A coupled closed-form/Doubly Asymptotic Approximation approach for the response of orthotropic plates subjected to an underwater explosion

Ye Pyae Sone Oo[a*], Hervé Le Sourne[b] and Olivier Dorival[c]

[a]*GeM Institute (UMR CNRS 6183) – Calcul-Meca, Nantes, France*
[b]*GeM Institute (UMR CNRS 6183) – Icam Nantes campus, France*
[c]*Clément Ader Institute (FRE CNRS 3687) – Icam Toulouse campus, France*

Abstract

In this paper, a closed-form analytical solution procedure is proposed to solve the coupled fluid-structure interaction (FSI) equations that involve the first-order Doubly Asymptotic Approximation (DAA_1) formulation. An efficient method comprised of the nonstandard finite difference (NSFD) scheme is applied. First of all, analytical equations are developed to analyze the response of a rigid mass-spring oscillator in an air-backed condition when it is subjected to a plane shock exponential wave coming from a far-field underwater explosion. After validating the results with LS-DYNA/USA (DAA_1), these equations are extended to determine the response of a two-dimensional, simply-supported rectangular plate, and then tested on the isotropic and orthotropic plates within a small deflection regime. Parametric studies are also performed by varying the load decay times, peak pressures, as well as the aspect ratios of the plate. Finally, the advantages and limitations of the proposed formulae are exposed along with suggestions for the future work.

Keywords: Doubly-Asymptotic Approximation (DAA); Fluid-structure interaction (FSI); Underwater explosion (UNDEX); LS-DYNA/USA; Nonstandard finite difference (NSFD) method.

1. Introduction

Non-contact underwater explosion (UNDEX) has long been a major threat to military vessels and civil marine structures since World War I and II. In order to prevent immersed structures against such intense loadings, it is very important for the designers to fully understand the underlying physics such as shock wave propagation, fluid-structure interaction (FSI), bulk cavitation, and so on. Over the past few decades, advanced numerical approaches involving Underwater Shock Analysis (USA) code have been widely used to analyze the underwater shock structure interaction problems. The fluid equations solved by USA code employ Doubly Asymptotic Approximation, a boundary element method proposed by (Geers 1978) during the 1970s. These are time domain differential equations that approach exactness at both low and high frequencies, allowing for a smooth transition in-between. The governing equations are expressed in terms of wet surface variables only and thus, it is not required to explicitly model the surrounding fluid. Traditionally, these equations have been solved using a staggered numerical solution procedure and been incorporated into various commercial finite element tools such as LS-DYNA, NASTRAN (DeRuntz 1989). These numerical tools are indeed very powerful. Nevertheless, as investigated by (Barras 2012), they can be computationally expensive and also demand much competence from the users. Consequently, they are not suitable for the preliminary design phases in which numerous loading scenarios as well as different structural configurations need to be tested. In this regard, simplified analytical solutions become more relevant since they provide reasonably accurate solutions in a relatively short amount of time as well as good insights to the problems.

* Corresponding author. Tel.: +33-0-240524827.
E-mail address: ye-pyae.sone-oo@icam.fr

Nomenclature

A_f	the (wetted) surface area of the plate
c_w	speed of sound in water (fluid)
h	thickness of the plate
I_0	applied impulse related to the incident wave
I_t	reduced transferred impulse due to the FSI effect
m, n	mode numbers in x- and y-directions respectively
M_f	water-added mass per unit area
m_s	areal mass of the plate
P_0	peak pressure
P_i	incident pressure
P_s	scattered pressure
ψ_x, ψ_y	rotations of the transverse normal about y- and x-axes respectively
P_{tot}	the total pressure acting on the plate
ρ_s	density of the plate
ρ_w	density of water (fluid)
t	time
τ	decay time of the loading
u_i	particle velocity of the incident wave
u_s	particle velocity of the scattered wave
v_i	impulsive velocity
w	transverse displacement

Underwater explosions not only generate a primary shock wave, which propagates through the surrounding fluid medium, but also cause the formation and oscillation of a gas bubble. Depending on the standoff distance and the charge mass, these can be characterized as near-field or far-field explosions. In this paper, it is assumed that the target plate is at a sufficiently far standoff distance from the explosive charge so that the pressure can be regarded as a plane shock wave and the secondary pressure wave caused by the bubble pulsation can be ignored. According to (Cole 1948), the plane shock pressure wave can be expressed as:

$$P(t) = P_0 e^{-t/\tau}, \quad for\ 0 \le t \le \tau \tag{1}$$

where P_0 is the peak pressure, t is the time variable, and τ is the decay time required for the peak pressure to fall to $1/e$ of its peak value. The corresponding peak pressure P_0 and the decay time τ can be determined from the charge mass C, standoff distance R and the type of the explosive charge by using the Principle of Similarity as follows (Cole 1948):

$$P_0 = K_1 \left(\frac{C^{1/3}}{R}\right)^{A_1}, \qquad \tau = K_2 C^{1/3} \left(\frac{C^{1/3}}{R}\right)^{A_2} \tag{2}$$

where K_1, A_1, K_2 and A_2 are constants that depend on the types of the explosives.

The arrival of the plane shock wave to the target structure would bring about an interaction phenomenon in which the total pressure at the interface can be obtained by a linear superposition of the incident and scattered pressures. The scattered pressure involves reflection of the incident pressure after the impact and damping radiation caused by the sudden movement of the plate. This is called high frequency or early-time interaction phenomenon and its solution was proposed by (Taylor 1941) in which the plate is either free-standing or supported by a linear spring. Taylor's theory, however, did not take into account the late-time phenomenon or the cavitation effect. The former effect can be associated to an additional pressure created during the plate deceleration phase while the latter should be accounted for when the total pressure in the fluid drops below the vapor pressure. Nevertheless, due to the simplicity and effectiveness of Taylor's solutions, there have been many research efforts in the past that used Taylor's FSI formulations to idealize the underwater blast as an impulsive loading, for example, (Hutchinson and Xue 2005; Brochard *et al.* 2018, 2020). The authors have also applied a similar approach by dividing the FSI response stages into two: early-time and long-time stages, see (Sone Oo *et al.* 2019).

However, this kind of approach may lead to overestimation or underestimation of the plate response according to (Deshpande *et al.* 2006; Schiffer *et al.* 2012). Recently, (Sone Oo *et al.* 2020) also investigated the applicability of the Taylor's 1D FSI theory in the study of underwater explosion response of the orthotropic plates. Based on various case studies, it was shown that the two-step approach based on Taylor's theory is valid only for a certain range of FSI parameter.

In this regard, Doubly Asymptotic Approximations developed by (Geers 1978) may be applied so as to alleviate some of the limitations imposed by the previous two-step approach. These are the first- and second-order differential equations in time to determine the fluid pressure due to scattered wave on the fluid-structure interface. They take into account both early- and long-time structural motions as well as a smooth transition between the two. The second-order approximation (DAA_2) is a generalization of the first-order approximation (DAA_1) with an enhanced accuracy. However, due to the increased complexity of DAA_2, only DAA_1 is adapted in this paper. The objective is to propose a closed-form like solution so that the coupled FSI equations of DAA_1 can be solved rapidly. This is done by adapting a nonstandard finite difference (NSFD) scheme developed by (Songolo and Bidégaray-Fesquet 2018). The use of NSFD scheme ensures the exactness of the solutions as will be seen in the next section. In what follows, analytical equations are derived to predict the response of an air-backed, spring-supported rigid plate. Then, they are extended for a 2D deformable, air-backed plate with simply-supported boundary condition. The obtained results are evaluated by comparing with those simulated in LS-DYNA/USA (DAA_1) with or without cavitation and also with the previous results available in (Sone Oo *et al.* 2020). Finally, the advantages and limitations of the proposed formulations are exposed, leaving grounds for future research.

2. Analytical models

2.1. Response of a spring-supported rigid plate

Suppose that a rigid plate having an areal mass m_s is subjected to a uniformly distributed incident shock wave $P_i(t)$. The plate is exposed to water with density ρ_w on one side and a linear spring and air on the other side, see Fig. 1. The equation of motion of a single degree-of-free (DOF) system can thus be written as:

$$\ddot{W}(t) + \omega^2 W(t) = \frac{P_{tot}(t)}{m_s} \tag{3}$$

where $m_s = \rho_s h$ is the areal mass of the plate; $\omega = \sqrt{K/m_s}$ is the angular frequency of the plate, K is the areal stiffness of the spring, $P_{tot}(t)$ is the total pressure acting on the plate (the evolution of total pressure is explained in Eqs. (4) and (5)), and $W(t)$ is the displacement of the plate taken positive in the z-direction as shown in Fig. 1.

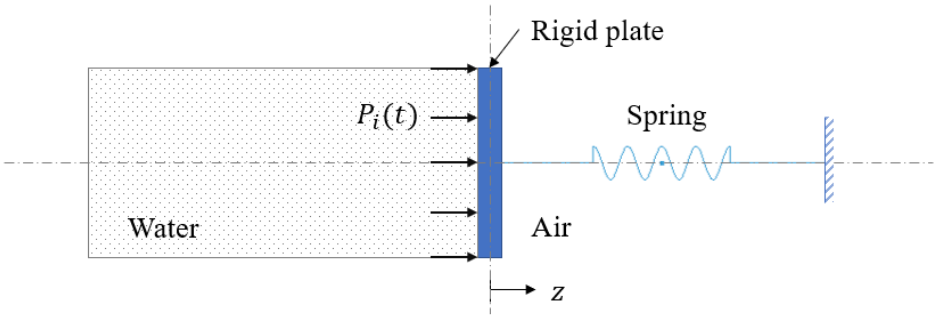

Fig. 1. A mass-spring system containing a rigid plate subjected to an incident pressure

The total pressure $P_{tot}(t)$ from Eq. (3) is determined by a linear superposition of the incident pressure $P_i(t)$ and the scattered pressure $P_s(t)$. Mathematically,

$$P_{tot}(t) = P_i(t) + P_s(t) \tag{4}$$

In this paper, the incident pressure is considered as an exponential decay form, Eq. (1). According to DAA$_1$ formulation of (Geers 1978), the scattered pressure $P_s(t)$ can be given as:

$$\dot{P}_s(t) + D_f P_s(t) = \rho_w c_w \dot{u}_s(t) \tag{5}$$

where $D_f = (\rho_w c_w)/(M_f)$ is the ratio of the acoustic impedance of water to the water-added mass per unit area of the submerged plate, and $\dot{u}_s(t) = \dot{u}_i(t) - \dot{W}(t)$ in which $\dot{u}_s(t)$ and $\dot{u}_i(t)$ are the incident and scattered accelerations of the fluid particles respectively. The expression for $\dot{u}_s(t)$ comes from the velocity continuity condition at the fluid-structure interface. M_f is the *areal* water-added mass for the rigid plate when it moves in water and can be calculated from (Blevin 1979).

Equation (5) is called 'Doubly-asymptotic' because it approaches exactness in both high and low frequencies. For high frequency motions, $|\dot{P}_s| \gg |P_s|$, and thus, Eq. (5) becomes $P_s(t) = \rho_w c_w u_s(t)$. For low frequency motions, $|\dot{P}_s| \ll |P_s|$ so that Eq. (5) shows the incompressible-flow relationship, $P_s = M_f \dot{u}_s$ (DeRuntz 1989). The system of equations becomes coupled when Eq. (5) is solved together with the structural equation, Eq. (3). The scattered pressure, particle acceleration, as well as the kinematics of the plate must be updated for each time step.

For a far-field plane shock wave, the incident pressure is related to the incident particle velocity as:

$$P_i = \rho_w c_w u_i \tag{6}$$

To discretize Eq. (3) in time domain, let us rearrange it into a system of two first-order differential equations as:

$$\begin{aligned} \dot{W} &= V \\ \dot{V} &= -\omega^2 W + \frac{P_{tot}}{m_s} \end{aligned} \tag{7}$$

Equation (7) can be expressed in matrix form as:

$$[\dot{X}] = [A][X] + [B] \tag{8}$$

where $[\dot{X}] = \begin{bmatrix} \dot{W} \\ \dot{V} \end{bmatrix}$, $[X] = \begin{bmatrix} W \\ V \end{bmatrix}$, $[A] = \begin{bmatrix} 0 & 1 \\ -\omega^2 & 0 \end{bmatrix}$ and $[B] = \begin{bmatrix} 0 \\ \frac{P_{tot}}{m_s} \end{bmatrix}$.

For the numerical approximation of Eq. (8), the interval $[t_0, t]$ is discretized into:

$$t^i = t_0 + (i-1)\Delta t \tag{9}$$

where the parameter $\Delta t > 0$ is the step size, t_0 is the initial time, t^i is the current time step, and $i = 1,2,3,\ldots$ refers to the discrete points in time. An approximate solution for $[X(t^i)]$ at time t^i is denoted here as $[X]^i$ for simplicity and can be obtained by applying an efficient numerical scheme called nonstandard finite difference (NSFD) methodology (Mickens 1993).

Definition 1. *The numerical solution for Eq. (8) is called a nonstandard finite difference method if at least one of the following conditions is satisfied:*

- *The renormalization of the step size:* $[\dot{X}]^i = \left(\phi(\Delta t)\right)^{-1}(X^{i+1} - X^i)$, *where* $\phi(\Delta t) = \Delta t I + \mathcal{O}(\Delta t^2)$ *is a positive diagonal matrix; and*
- *The nonlocal approximation of the right-hand side of Eq. (8): for example,* $[X] \to [X]^{i+1}$.

(Mickens 1993)

If $[B]$ from Eq. (8) is taken as zero, the exact numerical solution is:

$$[X]^{i+1} = \left\{e^{[A]\Delta t}\right\}[X]^i \tag{10}$$

With some algebraic manipulations, it is able to show that:

$$[\phi(\Delta t)]^{-1}([X]^{i+1} - [X]^i) = [A][X]^i \tag{11}$$

where $[\phi(\Delta t)] = \left(\left[e^{[A]\Delta t}\right] - I\right)[A]^{-1}$ which satisfies the first condition of **Definition 1** on NSFD scheme. By adding the non-autonomous term to Eq. (11), the scheme becomes:

$$[\phi(\Delta t)]^{-1}([X]^{i+1} - [X]^i) = [A][X]^i + [B]^i \tag{12}$$

whose explicit form including the matrix $\left\{e^{[A]\Delta t}\right\}$ is as follows:

$$[X]^{i+1} = \left\{e^{[A]\Delta t}\right\}[X]^i + [\phi(\Delta t)][B]^i \tag{13}$$

The solution to Eq. (13) lies in finding the exponential matrix $\left\{e^{[A]\Delta t}\right\}$ which can be done by using the following linear combination (Songolo and Bidégaray-Fesquet 2018):

$$\left\{e^{[A]\Delta t}\right\} = \left(\frac{\lambda_1 e^{\lambda_2 \Delta t} - \lambda_2 e^{\lambda_1 \Delta t}}{\lambda_1 - \lambda_2}\right)[I] + \left(\frac{e^{\lambda_1 \Delta t} - e^{\lambda_2 \Delta t}}{\lambda_1 - \lambda_2}\right)[A] \tag{14}$$

where $\lambda_1, \lambda_2 = \pm\omega$ are two distinct eigenvalues of the $[2 \times 2]$ matrix $[A]$. By substituting them in Eq. (14), the expression for exponential matrix $\left\{e^{[A]\Delta t}\right\}$ is obtained. Then, the resulting matrix is introduced into Eq. (13), leading to the closed-form like expressions below:

$$\begin{aligned} W^{i+1} &= W^i \cos(\omega\Delta t) + V^i \left(\frac{\sin(\omega\Delta t)}{\omega}\right) - P_{tot}^i \left(\frac{\cos(\omega\Delta t) - 1}{m_s \omega^2}\right) \\ V^{i+1} &= -W^i \omega \sin(\omega\Delta t) + V^i \cos(\omega\Delta t) + P_{tot}^i \left(\frac{\sin(\omega\Delta t)}{m_s \omega}\right) \end{aligned} \tag{15}$$

where the step size required to solve these explicit equations is estimated as $\Delta t \leq \pi/(200\omega)$, which is at most one-hundredth of the time to reach the first peak displacement. It is worth mentioning here that these closed-form like expressions ensure the exactness of the solution and can be readily solved for any initial conditions at time step t^i. Unlike the well-known Runge-Kutta scheme, the present scheme does not require additional function evaluations, thus saving more computation time, as will be shown later.

Applying the same procedure on Eq. (5), the expression for P_s for the next time step is obtained as:

$$P_s^{i+1} = P_s^i e^{-D_f \Delta t} + \left(\frac{1 - e^{-D_f \Delta t}}{D_f}\right)\left(-\rho_w c_w \dot{V}^i + \dot{P}_i^i\right) \tag{16}$$

Since the incident pressure P_i is known for all time steps, total pressure P_{tot} can be updated for each time step if Eq. (16) is solved simultaneously using Eqs. (4) and (15). The initial conditions at time step zero are taken as $W(0) = V(0) = 0$, $\dot{V}(0) = 2P_0/m_s$ and $P_s(0) = P_i(0) = P_0$. Note that cavitation can be considered by introducing a flag that would trigger whenever $P_{tot}^i \leq 0$. Following the suggestion of USA user's manual (LSTC, 2017b), only the scattered pressure P_s is modified whenever the cavitation criterion is met.

2.2. Response of a 2D deformable simply-supported plate

The mass-spring equation from the previous subsection is extended to determine the response of an air-backed rectangular plate in a simply-supported boundary condition when subjected to a plane shock wave in a negative z-direction, see Fig. 2. The plate is assumed to have the size (a, b) and a uniform thickness h. Cartesian coordinate system is employed with the origin being located at the corner and mid-surface of the plate. Each k^{th} ply is rotated an arbitrary angle θ^k with respect to the x-axis as shown. The first-order shear deformation theory (FSDT) is applied together with the Lagrangian equations to

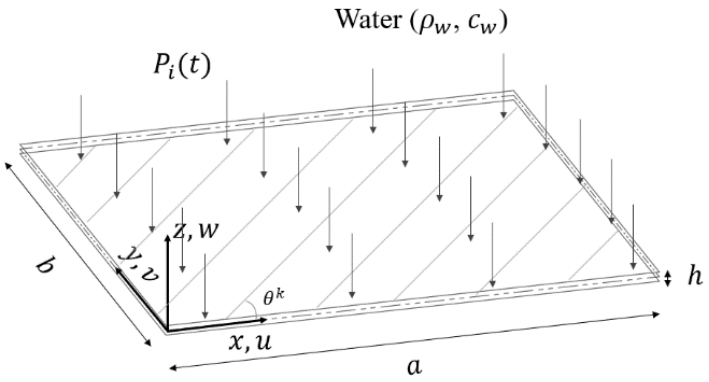

Fig. 2. Coordinate system and geometry of the rectangular plate

derive the equations of motion for the plate. In this paper, only a brief account of these derivations is presented. For further details, the readers are referred to (Sone Oo *et al.* 2019, 2020).

According to FSDT, the following assumptions are made to derive the mechanical model of the plate:

- The transverse displacement is assumed to be independent of the thickness and the transverse normal strain is taken as zero.
- The transverse normal is allowed to rotate with respect to the mid-surface after the deformation.
- Stress-strain relations obey generalized Hooke's law for orthotropic materials.
- Linear strain-displacement relations are considered.
- In-plane displacements are assumed negligibly small compared to the transverse displacement, i.e. $|u|, |v| \ll |w|$, thus reducing the problem from 5 degrees of freedom (DOFs) to 3 DOFs.
- In-plane and rotatory inertia are assumed negligibly small.
- Hydrostatic pressure, structural damping and the effect of failure are not considered.

To satisfy the simply-supported boundary conditions, Navier solution functions consisting of double Fourier summation can be adapted:

$$w(x,y,t) = \sum_{m=1}^{\infty}\sum_{n=1}^{\infty} W_{mn}\, sin\left(\frac{m\pi x}{a}\right) sin\left(\frac{m\pi y}{b}\right) \tag{17a}$$

$$\psi_x(x,y,t) = \sum_{m=1}^{\infty}\sum_{n=1}^{\infty} \Psi_{x_{mn}}\, cos\left(\frac{m\pi x}{a}\right) sin\left(\frac{m\pi y}{b}\right) \tag{17b}$$

$$\psi_y(x,y,t) = \sum_{m=1}^{\infty}\sum_{n=1}^{\infty} \Psi_{y_{mn}}\, sin\left(\frac{m\pi x}{a}\right) cos\left(\frac{m\pi y}{b}\right) \tag{17c}$$

where W_{mn}, $\Psi_{x_{mn}}$ and $\Psi_{y_{mn}}$ are three generalized coordinates, m and n are mode numbers in x- and y-directions respectively.

The time domain equation of motion for mode (m,n) of the plate is as follows:

$$\ddot{W}_{mn}(t) + \omega_{mn}^2 W_{mn}(t) = \frac{4}{A_f m_s} F_{mn}(t) \tag{18}$$

where $A_f = ab$ is the wet surface area of the plate, and the modal participation of the forcing term on the right-hand side of Eq. (18) can be expressed in terms of incident and scattered pressures as:

$$F_{mn}(t) = \int_0^b \int_0^a \left[\left(P_i(t) + P_s(x,y,t)\right) sin\left(\frac{m\pi x}{a}\right) sin\left(\frac{m\pi y}{b}\right)\right] dx\, dy \tag{19}$$

where the natural frequency is $\omega_{mn} = \sqrt{K_{mn}/m_s}$, see Eq. (A1) of Appendix A to find the formulations of K_{mn}.

Note that the incident pressure is assumed to be evenly distributed across the plate and thus, does not depend on spatial coordinates. However, the scattered pressure is both a function of spatial and temporal variables. Assuming that the scattered pressure has the same mode shape functions as the transverse displacement, then

$$P_s(x,y,t) = \sum_{m=1}^{\infty}\sum_{n=1}^{\infty} p_{mn}\, sin\left(\frac{m\pi x}{a}\right) sin\left(\frac{n\pi y}{b}\right) \tag{20}$$

In this case, a further assumption is imposed where DAA_1 from Eq. (5) is modified into:

$$\dot{P}_s(x,y,t) + D_f P_s(x,y,t) = \rho_w c_w(\dot{u}_i(t) - \ddot{w}(x,y,t)) \tag{21}$$

Substituting Eq. (20) into Eq. (21), multiplying both sides with the mode shape functions and then integrating both sides with respect to the surface area, the modal equation for the scattered pressure can be derived. On virtue of the orthogonality of the modes:

$$\int_0^b \int_0^a (\,\alpha_{mn}\alpha_{rs}\,)\, dx\, dy = \begin{cases} \frac{A_f}{4}, & \text{if } m,n = r,s \\ 0, & \text{if } m,n \neq r,s \end{cases} \tag{22}$$

where $\alpha_{mn} = \sin(m\pi x/a)\sin(n\pi y/b)$, $\alpha_{rs} = \sin(r\pi x/a)\sin(s\pi y/b)$, and $m,n,r,s = 1,3,5,\ldots$ for the bi-symmetric problem (that is, symmetries in both x- and y-axes).

The fluid modal equation derived using Eq. (21) is:

$$\dot{p}_{mn}(t) = -D_{f_{mn}} p_{mn}(t) - \rho_w c_w \ddot{W}_{mn}(t) + \left(\frac{16}{mn\pi^2}\right)\dot{P}_i(t) \tag{23}$$

Then, the force function from the right-hand side of Eq. (18) becomes:

$$F_{mn}(t) = \left(\frac{4A_f}{mn\pi^2}\right) P_i(t) + \left(\frac{A_f}{4}\right) p_{mn}(t) \tag{24}$$

Using the same steps shown in the previous subsection, the following explicit equations are derived:

$$W_{mn}^{i+1} = W_{mn}^{i}\, cos(\omega_{mn}\Delta t) + V_{mn}^{i}\left(\frac{sin(\omega_{mn}\Delta t)}{\omega_{mn}}\right) - 4F_{mn}^{i}\left(\frac{cos(\omega_{mn}\Delta t)-1}{A_f m_s \omega_{mn}^2}\right) \tag{25a}$$

$$V_{mn}^{i+1} = -W_{mn}^{i}\omega_{mn}\, sin(\omega_{mn}\Delta t) + V_{mn}^{i}\, cos(\omega_{mn}\Delta t) + 4F_{mn}^{i}\left(\frac{sin(\omega_{mn}\Delta t)}{A_f m_s \omega_{mn}}\right) \tag{25b}$$

$$\dot{V}_{mn}^{i+1} = -\omega_{mn}^2 W_{mn}^{i} + \frac{4}{A_f m_s} F_{mn}^{i} \tag{25c}$$

$$p_{mn}^{i+1} = p_{mn}^{i} e^{-D_{f_{mn}}\Delta t} + \left(\frac{1-e^{-D_{f_{mn}}\Delta t}}{D_{f_{mn}}}\right)\left(-\rho c \dot{V}_{mn}^{i} + \rho c \dot{u}_i^{i}\left(\frac{16}{mn\pi^2}\right)\right) \tag{25d}$$

in which the initial conditions are taken the same as the previous rigid plate-spring system, i.e., $W(0) = V(0) = 0$, $\dot{V}(0) = 2P_0/m_s$ and $P_s(0) = P_i(0) = P_0$. Here, the constant term $D_{f_{mn}} = \rho_w c_w / M_{f_{mn}}$ should be calculated for each mode (m,n).

The water-added mass $M_{f_{mn}}$ is calculated using (Greenspon 1961)'s formulation as follows:

$$M_{f_{mn}} = \frac{1}{2}\rho_w b f(a/b) A_{mn}^2 \tag{26}$$

where $f(a/b) = 1.5(a/b)^3 - 3.12(a/b)^2 + 2.6(a/b) + 0.0098$ is the correction term for aspect ratios of the plate ($0 < f(a/b) \leq 1$) for $a \leq b$, and $A_{mn} = 8/(mn\pi^2)$ is the modal term (consisting of only odd numbered modes) for simply-supported boundary conditions. This added-mass formulation contains some approximations on the mode shape term and hence, is accurate only for the first mode shape and $A_{mn} = 0$ for even numbered modes.

The modal terms after solving Eqs. (25a) – (25d) are substituted into Eq. (17). Then, FSDT solution for the UNDEX response of a simply-supported rectangular orthotropic plate is obtained.

3. Preliminary results and analyses

The analytical equations from Section 2 are implemented in a MATLAB program (version R2015a). The obtained results are then confronted to those calculated by LS-DYNA/USA (DAA_1) and the theoretical solutions using Taylor's formulation (Taylor 1941). Three different types of problems are studied: (1) spring-supported rigid plate subjected to a plane shock exponential wave, (2) simply-supported steel plate subjected to a uniformly distributed suddenly applied pressure load, and (3) simply-supported composite plate subjected to an exponentially decaying plane shock wave. Details about the finite element models are specified in each corresponding subsection.

3.1. Spring-supported rigid plate subjected to a plane shock exponential wave

A square rigid plate having the dimensions ($a = b = 167$ mm), uniform thickness ($h = 10$ mm), and density ($\rho_s = 1500$ kg.m^{-3}) is exposed to the water ($\rho_w = 1000$ kg.m^{-3}, c_w = 1498 m.s^{-1}) on one side. Four discrete springs possessing equivalent stiffness of $K = 4.5$ MN.m^{-1} are used to support the plate at corner nodes and on the other side of the plate. A single finite element rigid plate-spring model, resembling to the one depicted in Fig. 1, is constructed in LS-DYNA/USA (DAA_1). No fluid elements are modeled since the plate is coupled to DAA boundary element. Fully-integrated shell element formulation together with rigid material is applied.

A plane shock exponential wave comprised of a peak pressure $P_0 = 75$ MPa and the decay time $\tau = 0.21$ ms is considered in the USA keyword input. Cavitation is treated approximately by limiting the total pressure at zero whenever it becomes negative (Hoo Fatt and Sirivolu 2017; Schiffer and Tagarielli 2015). Here, both results with and without cavitation are shown for the comparison purpose. It should, however, be kept in mind that the treatment of cavitation on the fluid-structure interface is only an approximate approach, as mentioned in (LSTC 2017b). Results are calculated again using closed-form like analytical expressions given in Eqs. (15) and (16) as well as analytical solution proposed by (Taylor 1941). Since the purpose is to test the validity of the developed equations, the same value of water-added mass retrievable from LS-DYNA/USA (DAA_1), $M_f/m_s = 6.25$, is used for the analytical calculation.

In Fig. 3, the results of displacement, velocity, acceleration, and normalized total pressure (P_{tot}/P_0) obtained from LS-DYNA/USA (DAA_1), analytical (DAA_1), and analytical (Taylor 1941) are plotted as a function of time and up to 4 ms. As can be seen in all the plots, the current analytical solutions are almost exactly the same as the numerical results using LS-DYNA/USA (DAA_1) with or without cavitation. The change in the behavior of the plate caused by cavitation can be clearly observed when the pressure has been cut-off at about 1.4 ms. The analytical solutions by Taylor's formulations are also included in order to highlight the improvement brought by the current DAA-based approach. The original formulation of Taylor considers the early-time motion and hence, the effect of water-added mass or cavitation is not included. Figure 3 evidently shows that Taylor's approach is accurate only for the early-time (high frequency) motion, for instance, the velocity, acceleration and total pressure profiles are comparable to the DAA-based solutions until about 32 μs which is approximately the same as the first appearance of cavitation on the fluid-structure interface. Due to the influence of the long-time effect, the solutions are no longer comparable after that time.

Here, it is also worth mentioning that the authors tested the analytical formulations using other types of loading (e.g., sinusoidal load), and also with different acoustic impedance (e.g., in air). In all the tests performed, excellent agreement is found between analytical and numerical methods involving DAA_1. Therefore, it can be concluded that the FSI coupling scheme works quite well for a single degree-of-freedom (DOF) system.

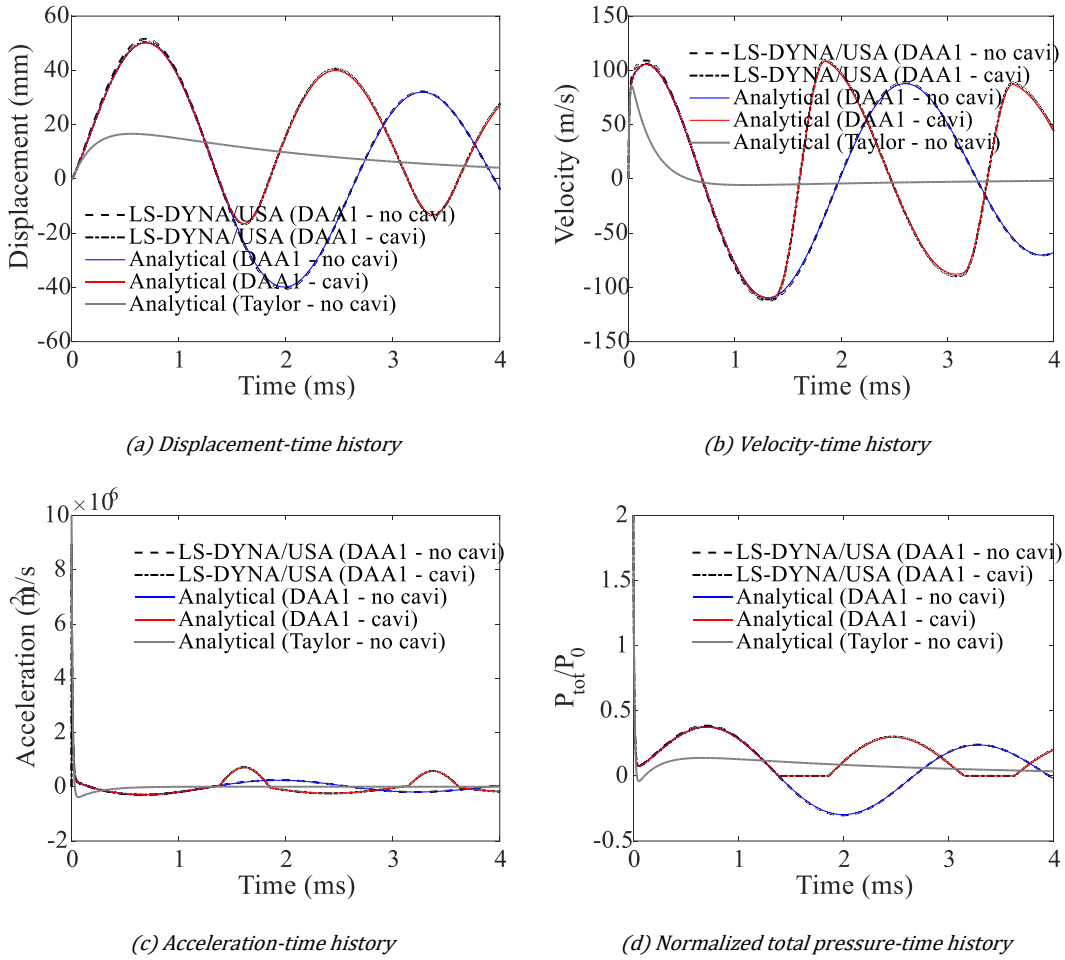

(a) Displacement-time history

(b) Velocity-time history

(c) Acceleration-time history

(d) Normalized total pressure-time history

Fig. 3. Comparison between LS-DYNA/USA (DAA$_1$), analytical solutions by Taylor's 1D FSI formulation and the present analytical results for 1 DOF system using DAA$_1$ formulations (with/without cavitation)

3.2. Simply-supported steel plate subjected to a uniformly distributed suddenly applied pressure load

For the verification purpose, a simple case study is performed by choosing a simply-supported isotropic (steel) plate subjected to a uniformly distributed suddenly applied pressure of 2.5 MPa. The characteristics of the steel plate are shown in Table 1. A quarter plate model ($50\ \text{mm} \times 50\ \text{mm}$) is constructed using a total of 169 fully-integrated shell elements along with the elastic material model (MAT_001) from LS-DYNA. Five through-thickness integration points are considered. A typical shear correction factor of 5/6 is applied. A symmetric boundary condition is imposed to the inner edges of the plate while simply-supported (immovable) boundary is prescribed on the outer edges. Structural damping, material strain rate and the plastic effects are not included, making sure that the deflection remains small. The plate is coupled to DAA$_1$ boundary elements by specifying wet surface segments on the plate. A uniformly distributed suddenly applied incident pressure (P_0 = 2.5 MPa), also known as 'step loading', is applied via USA keyword input. Cavitation is not considered in this analysis. The acoustic properties of water are taken as $\rho_w = 1025\ \text{kg.m}^{-3}$ and $c_w = 1500\ \text{m.s}^{-1}$.

Table 1. Characteristics of the isotropic (steel) plate

$a = b$ (mm)	h (mm)	ρ_s (kg.m^{-3})	E (GPa)	ν	σ_y (MPa)
100	5.76	7800	200	0.3	240

The results of the central deflection, velocity, acceleration and normalized total pressure are plotted as a function of time in Fig. 4. Four different results, namely, LS-DYNA/USA (DAA$_1$), analytical (DAA$_1$), analytical (Taylor 1D rigid) and analytical (Taylor 2D) are compared. The present analytical (DAA$_1$) solutions include 36 modal participation terms, i.e., $m, n = 1, 3, 5, \ldots, 11$ (or $M = N = 6$). The general trends of both time history plots agree well with LS-DYNA/USA (DAA$_1$). The peak deflection from LS-DYNA/USA (DAA$_1$) evaluated at the center of the steel plate shows 4% discrepancy with respect to the analytical (DAA$_1$) peak value. They show oscillatory nature with decreasing amplitudes due to the presence of the fluid. On contrary, the other two analytical results that consider Taylor's formulation (Taylor 1941) show completely different nature. The main difference between these two is that Taylor's 1D rigid formulation supposes a rigid plate backed by a linear spring while Taylor's 2D formulation is an extension of the 1D rigid plate to the 2D deformable plate model. The 2D version of the Taylor's theory has already been adapted by (Hoo Fatt and Sirivolu 2017). Obviously, 2D theory improves the result in the early-time (up to 0.1 ms). Nevertheless, due to the negligence of the long-time fluid-structure coupling, results of Taylor's theory are comparable only up to a certain time step (0.04 ms for 1D theory and 0.1 ms for 2D) as shown in Fig. 4. Response of the plate that uses DAA-based approaches are more physical in the sense that they show both the early- and long-time phenomena.

In Fig. 4 (c) and (d), oscillations can be seen in the acceleration and total pressure-time histories from the analytical (DAA$_1$) approach (red color lines). These can be explained through the insufficient water-added mass values in the present analytical (DAA$_1$) formulations especially when higher vibration modes are involved. According to Eq. (23), the scattered pressure depends on the constant D_{fmn} (recall that $D_{fmn} = \rho_w c_w / M_{fmn}$). The smaller M_{fmn} becomes, the larger the value of D_{fmn} is, leading to higher rate of change in the modal terms of the scattered pressure, i.e., $\dot{p}_{mn}$. The detailed studies as well as the improvement regarding the (areal) water-added mass calculations can be found in Section 4.

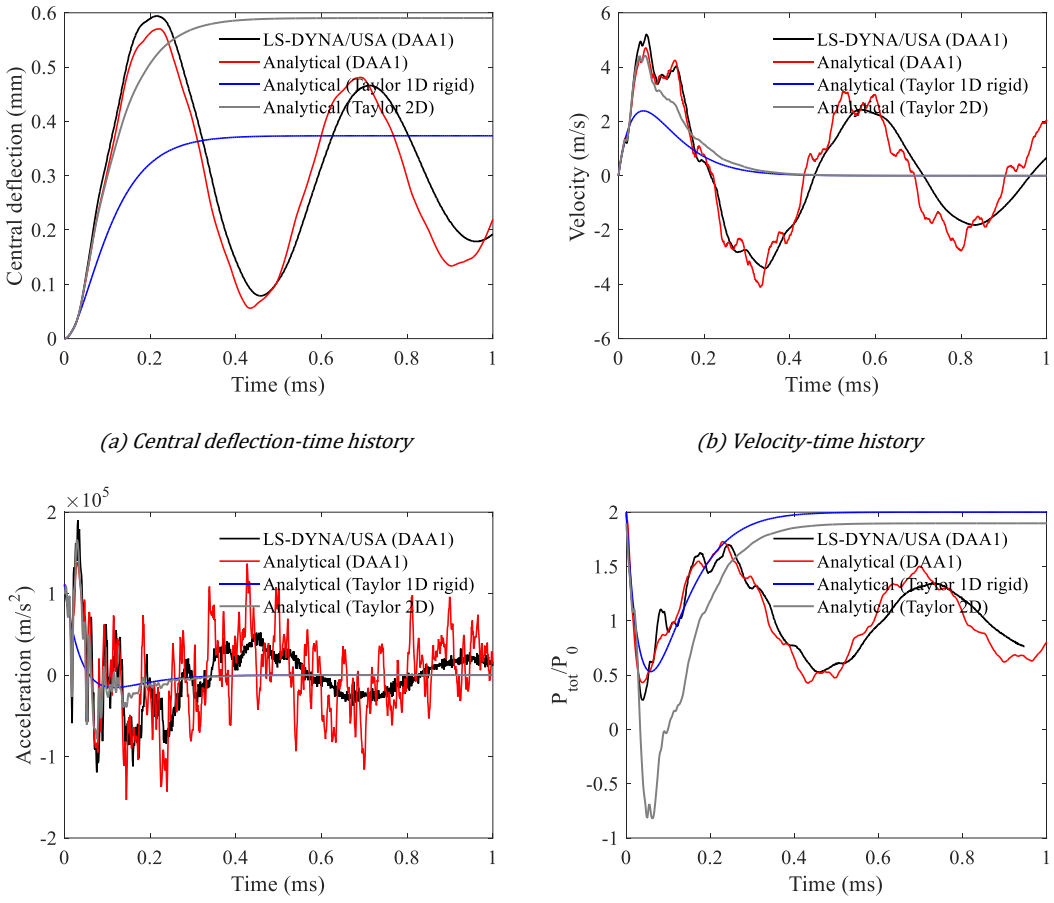

(a) Central deflection-time history

(b) Velocity-time history

(c) Acceleration-time history

(d) Normalized total pressure-time history

Fig. 4. Preliminary comparison of isotropic (steel) plate response between LS-DYNA/USA (DAA1), the present analytical (DAA1) approach, analytical (Taylor's 1D rigid plate), analytical (Taylor 2D) formulations (Step loading: $P_0 = 2.5$ MPa)

3.3. Simply-supported composite plate subjected to an exponentially decaying plane shock wave

A carbon-fiber/epoxy (CFRP) laminated plate having the same dimensions and thickness as the previous steel plate ($a = b = 100$ mm, $h = 5.76$ mm), and material density of 1548 kg.m^{-3} is considered here. The laminate consists of 20 plies with the stacking sequence of $[\pm 45/0/0/0/\pm 45/0/0/0/90/90]_S$, each ply having about 0.288 mm thickness. The material characteristics of the lamina used in CFRP plate are retrieved from the quasi-static tests performed by the authors, see Table 2. Only a quarter of the plate is modeled using symmetric boundary conditions. Simply-supported boundary conditions are applied to the plate's (outer) edges. The model employs 169 modified fully-integrated shell elements (EQ: -16) along with the composite material model (MAT_054), see (LSTC 2017a). Again, structural damping as well as damage effects are ignored in this analysis. An exponential incident shock wave having a peak pressure P_0 = 1.5 MPa and decay time τ = 1.3 ms is applied through DAA boundary elements. Note that this is the case where the effect of cavitation is supposed to be minimum since the load duration is relatively long compared to the plate (in-air) response time, i.e, $\tau/T_0 \approx 15$, where $T_0 = 1/(4f_0) = 86\ \mu s$. The acoustic properties of water are taken as $\rho_w =$ 1025 kg.m^{-3} and $c_w =$ 1500 m.s^{-1}. The authors have checked the mesh size sensitivity and the current result shown in this paper is the already converged one. In addition, the sensitivity studies regarding the numerical damping (Rayleigh damping) using LS-DYNA/USA (DAA$_1$) are performed, see Fig. B1 in Appendix B. It was found out that a recommended damping coefficient by LS-DYNA user's manual (LSTC 2017a) between 0.1 – 0.25 yields nearly identical results. Using a damping coefficient of 0.25, however, introduces some numerical instability.

Figure 5 shows the time evolutions of central-deflection, and normalized total pressure at the center of the plate. Five different results are plotted together. Numerical results obtained from LS-DYNA/USA (DAA$_1$) are with/without the cavitation whereas all other analytical solutions are without cavitation. It can be seen that the effect of cavitation is not significant in this case study since the two numerical results with/without cavitation are nearly identical.

Analytical (DAA$_1$) results involve 144 modes $(M, N) = (12, 12)$. The results are more or less the same as those that use $(M, N) = (6, 6)$. It should be kept in mind that the number of modes participating could have slight effects on the scattered pressure results as shall be discussed in Section 4. The authors also checked the sensitivity on the time step as well as shear correction factor on the analytical results. The results shown here used a time step of 0.1 μs, which is less than one-hundredth of the in-air swing time ($T_0/100 \approx 0.86\ \mu s$) and the (total) shear correction factor used is 5/6.

In Fig. 5(a), the peak deflection of the proposed analytical DAA-based approach is found to be about 0.32 ms and in good accordance with the numerical results. However, the period is slightly shorter for the analytical (DAA$_1$) result than that of LS-DYNA/USA (DAA$_1$). The oscillations in the normalized pressure-time history are clearly visible too. As have already been explained, this is mainly due to the discrepancy in the water-added mass calculation between analytical and numerical results. LS-DYNA/USA (DAA$_1$) is found to have a larger water-added mass compared to the water-added mass given by (Greenspon 1961), with a relative error of about 12% for mode [1,1]. These will be elaborated in the next section when natural frequencies up to the first four bending modes are compared in Table 3.

All of the solutions given by Taylor's theory in Fig. 5 are underestimated compared to DAA-based solutions. The plate reaches the peak displacement and the total pressure rises again due to the decrease of the velocity. Consequently, it would take quite some time for the plate to return to its original configuration. Taylor's solution is only accurate up to 15 μs as can be seen in Fig. 5(b). Similar to the previous case studies, the use of DAA-based solution approach improves Taylor's early-time FSI theory and yields more physical response in the longer-time.

Table 2. Characteristics of the carbon-fiber/epoxy lamina

E_{11} (GPa)	$E_{22} = E_{33}$ (GPa)	$\nu_{12} = \nu_{13}$	ν_{23}	$G_{12} = G_{13}$ (GPa)	G_{23} (GPa)
138	8.98	0.281	0.385	3.66	3.24

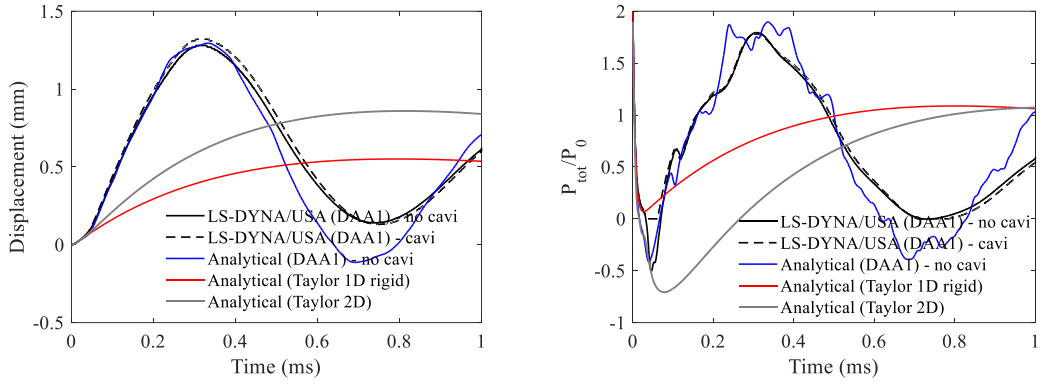

(a) Displacement-time history *(b) Normalized total pressure-time history*

Fig. 5. Comparison between LS-DYNA/USA (DAA$_1$) with/without cavitation, analytical (DAA1), analytical (Taylor 1D rigid) and analytical (Taylor 2D) results for the response of CFRP plate subjected to a plane shock wave (P_0 = 1.5 MPa, and τ = 1.3 ms)

4. Investigations and improvement on the water-added mass formulation

4.1. Modification

The original water-added mass formulation proposed by (Greenspon 1961) assumed that the plate is made up of many small rectangular elements with equal area. The average pressure on a point caused by the vibration of any other points on the plate is approximated by supposing that the entire plate acts as a rectangular piston with a deflection equal to the average of the spatial term $\alpha_{mn}(x,y)$. It was mentioned in the paper that such approximation is valid only for the first mode of the plate. According to Eq. (26), the water-added mass (per unit area) depends on the size and aspect ratio of the plate, the density of water and the square of the mode shape term A_{mn}^2. Therefore, to improve the formulation for higher modes, it can be reasoned that the term A_{mn}^2 from Eq. (26) should be modified. Recall that,

$$A_{mn}^2 = \frac{64}{m^2 n^2 \pi^4} \tag{27}$$

which is independent of each mode. In this paper, by combining the modal index (m,n) from each direction x and y, Eq. (27) is modified as a summation form as $A_{mn}^2 = \sum_{j=1}^{\infty} 64/(mnj^2\pi^4)$, where $j = 1,3,5,\ldots$ is the odd numbered modal index. Note that the idea of adapting the summation form in calculating A_{mn}^2 is only an approximate attempt to slightly increase the value of the areal water-added mass at every mode. Hence, Eq. (26) becomes:

$$M'_{f\,mn} = \frac{1}{2}\rho_w b f(a/b) \sum_{j=1}^{\infty} \frac{64}{mnj^2\pi^4} \tag{28}$$

Here, only the first 6 terms ($j = 1,3,\ldots,11$) are considered in the calculation of water-added mass. Since j^2 is in the denominator, using higher values of j in the series would not change the final result by a lot, as shall be shown.

In Fig. 6, the previous results on CFRP plate and the improved results using Eq. (28) are compared. LS-DYNA/USA (DAA$_1$) results are also plotted as reference. It can be seen that the small oscillations in the normalized total pressure-time plot disappear and the period of oscillation becomes more comparable to LS-DYNA/USA (DAA$_1$). As explained before, the increase in $M_{f_{mn}}$ would result in the decrease of $D_{f_{mn}}$ which in turn leads to smaller rate of change in the scattered pressure result according to Eq. (23). In Fig. 6, it can be seen that the improvement causes only slight changes to the central deflection results.

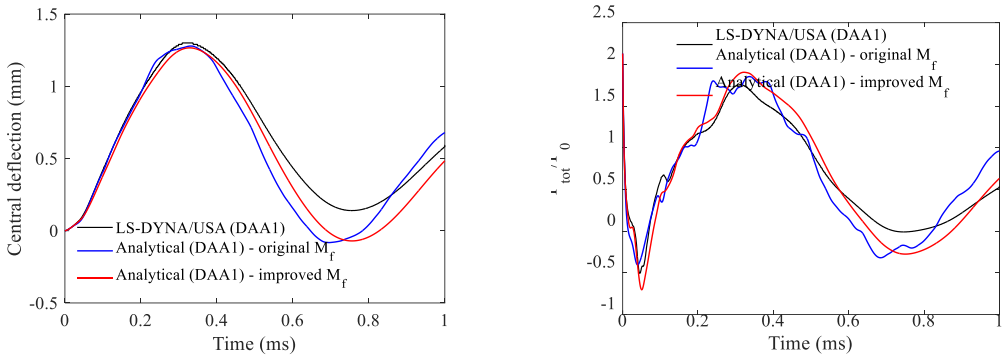

(a) Central deflection-time history *(b) Normalized total pressure-time history*

Fig. 6. Comparison between original and improved formulations of water-added mass (using CFRP plate subjected to an exponential loading of $P_0 = 1.5$ *MPa and* $\tau = 1.3$ *ms)*

4.2. Evaluations of the natural frequencies

Comparison of natural frequencies (both in-air and in-water) up to the first four bending modes is given in Table 3. Note that the inclusion of water-added mass decreases the in-air natural frequencies to half or even more than half in some cases. It can be seen that using the improved formulation of water-added mass, Eq. (28), could bring an improvement to the natural frequencies of the steel and composite plates compared to the original water-added mass formulation given by (Greenspon 1961).

Table 3. Comparison of natural frequencies (up to the first four bending modes)

			Natural frequencies in-air			Natural frequencies in-water			Discrepancy	
Material	a/h	Mode	Analytical	Numerical	Discrep.[1]	Numerical	Ana. original[2]	Ana. improved[3]	Original	Improved
			Hz	Hz	%	Hz	Hz	Hz	%	%
Steel	69	[1,1]	173	173	0.1%	80	87	81	8%	1.7%
		[1,3]	864	870	-0.7%	585	748	584	22%	-0.3%
		[3,1]	864	870	-0.7%	585	748	584	22%	-0.2%
		[3,3]	1552	1553	-0.1%	1174	1524	1313	23%	11%
	17	[1,1]	2747	2736	1.1%	1953	2077	1997	6%	2.2%
		[1,3]	13258	13420	-0.9%	11653	12738	11638	9%	-0.1%
		[3,1]	13258	13427	-1.0%	11653	12738	11638	9%	-0.1%
		[3,3]	23087	22971	-0.1%	21185	22981	22020	8%	3.8%
CFRP	69	[1,1]	191	190	0.5%	43	48	44	10%	2.7%
		[1,3]	673	669	0.6%	259	411	254	37%	-1.9%
		[3,1]	1220	1216	0.3%	472	745	461	37%	-2.4%
		[3,3]	1672	1652	1.2%	754	1535	965	51%	22%
	17	[1,1]	2906	2807	3.4%	1172	1330	1239	12%	5.4%
		[1,3]	9620	9431	2.0%	6037	8074	6083	25%	0.8%
		[3,1]	14661	14456	1.4%	9258	12305	9271	25%	0.1%
		[3,3]	19518	18965	2.8%	13546	19078	15935	29%	15%

[1] *where all the discrepancies are calculated using the formula,* $Discrep. = \frac{Analytical - Numerical}{Analytical} \times 100\%$.

[2] *Ana. original - Analytical calculation using original water-added mass formulation proposed by* (Greenspon 1961)*, Eq. (26).*

[3] *Ana. improved - Analytical calculation using improved water-added mass formulation, Eq. (28).*

4.3. Sensitivity to the number of mode shapes

The use of summation form in the water-added mass calculation in Eq. (28) does not make a closed-form expression, and thus, the effect of the number of modal terms is investigated. The case with a steel plate model defined in Subsection 3.2 is used in this case. As plotted in Fig. 7, using different number of modal terms does not change the results a lot. In fact, the central deflections are almost identical. The normalized scattered pressures are only slightly affected at the beginning of the calculation. According to the initial condition, the scattered pressure at time $t = 0$ should be $P_s(0) = P_0$. However, The Fourier series decomposition of P_s shown in Eq. (20) could satisfy such a condition only after taking into account several modes, for instance, $M = N = 30$. Even so, the overall behavior in the longer time converges regardless of the number of modes ($M, N \geq 3$) according to the results shown.

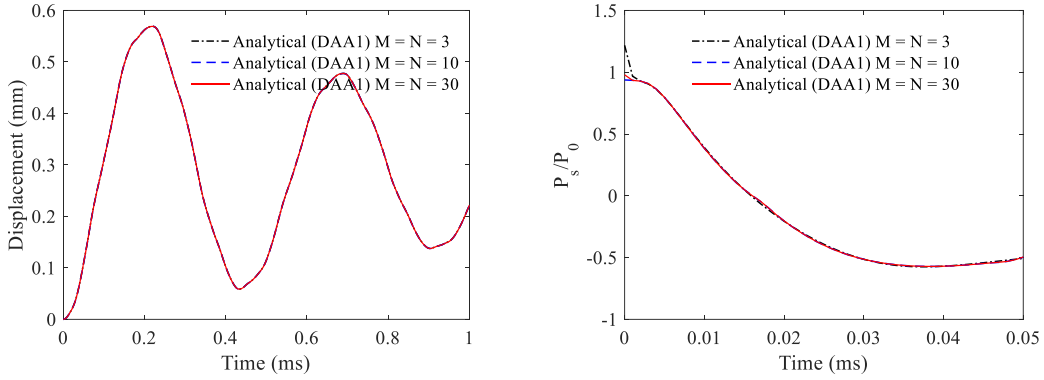

(a) Central deflection-time history *(b) Normalized scattered pressure-time history*

Fig. 7. Effect of the number of modal terms in analytical (DAA_1) approach (using steel plate, step loading of 2.5 *MPa)*

5. Parametric studies

In this section, the effect of changing the aspect ratios as well as the loading is studied using the material models presented before. The problem domain is divided into two: (1) steel plate responses under varying levels of step loadings, and (2) composite plate responses under different exponential loadings. Two different sizes of the plate are adapted and termed as 'thin' plate and 'thick' plate. Thin plate has the dimension of $a = b = 400$ mm while thick plate possesses $a = b = 100$ mm. Same thickness of 5.76 mm is used in all cases to keep the same areal mass. As before, cavitation or damage is not included in the study. Note also that an improved water-added mass formulation, Eq. (28), and up to 36 modal terms ($M = N = 6$) are considered in all the coming analyses.

5.1. Steel plate responses under varying levels of step loadings

In Fig. 8, maximum central deflection-thickness ratios (w_{max}/h) for thin and thick steel plates are plotted as a function of the step pressures P_0, ranging 10 – 100 kPa for thin plate and 2 - 24 MPa for thick plate. As expected, the analytical (DAA_1) results are linearly proportional to the peak pressures and valid until the geometric nonlinearity caused by large deflection takes effect. It can be seen in Fig. 8(a) that such effect is more significant for thin plate (large a/h ratio) due to its lower stiffness. The thick plate (small a/h ratio) appears to withstand linearly much higher pressures accompanied by lower w_{max}/h results. A relative error of $\pm 15\%$ (with respect to the analytical results) is shown in both plots. It can be said that the current analytical (DAA_1) results correlate well with those of LS-DYNA/USA (DAA_1) up to $w_{max}/h \leq 0.5$. To exceed this value, it would be necessary to incorporate geometric nonlinear effect (by moderate rotation or large deflection) into the formulations.

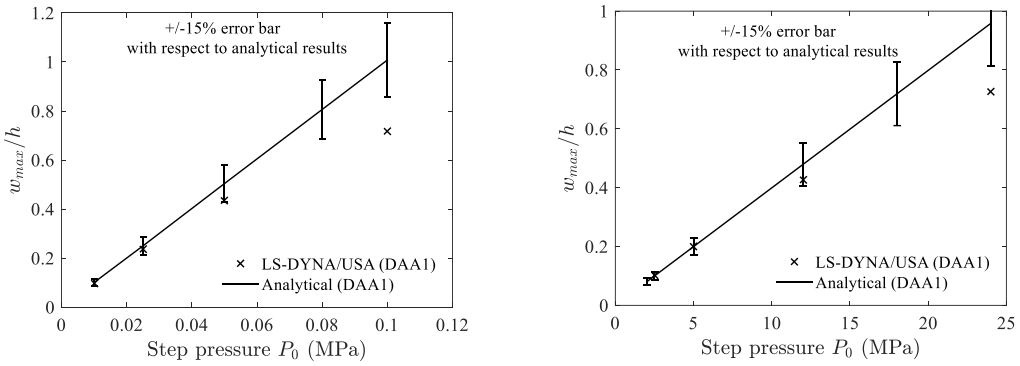

(a) Thin steel plate ($a/h = 69.4$) *(b) Thick steel plate ($a/h = 17.4$)*

Fig. 8. Comparison of the responses of (a) thin steel plate ($a/h = 69.4$), and (b) thick steel plate ($a/h = 17.4$) loaded by varying levels of suddenly applied step pressures using LS-DYNA/USA (DAA_1) and analytical (DAA_1) approaches

5.2. Composite plate responses under different exponential loadings

5.2.1. Sensitivity to varying the peak pressure P_0

Thick CFRP plate, whose material characteristics are given in Table 2, is subjected to varying levels of peak pressures ($P_0 = 0.75$ - 2.6 MPa) while keeping the same decay time ($\tau = 1.3$ ms) from Subsection 3.3. Since the decay time of the applied loading is relatively higher than the in-air plate response time ($T_0 \approx 1/(4f_0) = 86$ μs), the effect of cavitation is expected to be minimum, recall Fig. 5(b). In addition, the resulting peak deflection is limited to be less than half the plate thickness so that evaluations can be made without the effect of the geometric nonlinearity due to large deflection.

In Fig. 9, maximum central deflections and peak strain energies obtained from three different approaches are compared, namely, (1) LS-DYNA/USA (DAA_1) without cavitation, (2) analytical (two-step) approach, and (3) analytical (DAA_1) approach without cavitation. Here, the analytical (two-step) approach is included just to highlight the improvements brought forth by the present analytical (DAA_1) model. In brief, analytical (two-step) approach consists of two calculation stages, namely, the early-time and long-time stages. During the early-time step, the maximum impulsive velocity to be transmitted to the plate is calculated, assuming a negligible deformation of the plate. Then, at the second step, the free response of the plate is determined, taking into account the water-added inertia effect. Important formulations of the two-step analytical approach are given in Appendix C for reference purpose.

As can be observed in Figs. 9(a) and (b), the analytical results with DAA_1 approach correlate quite well with the LS-DYNA/USA (DAA_1) results in both maximum central deflections and the peak strain energies. Relative discrepancy is found to be within $\pm 10\%$ only. On the other hand, the results of analytical (two-step) approach underestimate in all cases because the transferred impulse considered in two-step analytical approach does not account for the continuing action of FSI, especially when the incident load duration is relatively long. In this regard, it can be said that the current analytical approach (with DAA_1) improves the shortcoming of the previous analytical (two-step) impulse model.

5.2.2. Sensitivity to varying the FSI parameter ψ

Analyses are performed again by using the various load cases defined in Table 4. Note that the charge masses C and the standoff distances R are selected in order to have the same transferred impulse I_t to the plate. According to (Taylor 1941), the transferred impulse can be given as:

$$I_t = 2P_0\tau\,\psi^{-\psi/(\psi-1)} \tag{29}$$

where $\psi = \rho_w c_w \tau / m_s$ is the FSI coefficient associated to impedance of water, decay time and areal mass of the plate.

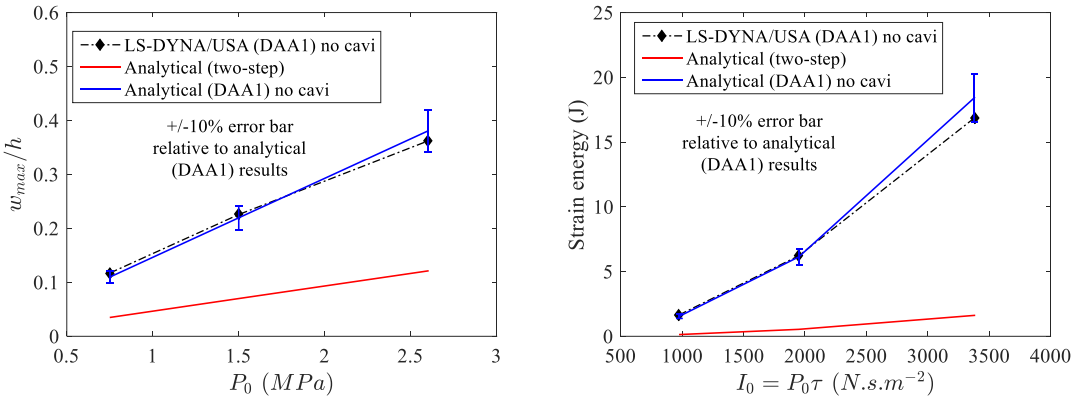

(a) Dimensionless peak deflection Vs applied pressures *(b) Strain energy Vs applied impulse*

Fig. 9. Sensitivity to varying the peak pressure P_0 *on thick CFRP plate* ($a/h = 17.4$) with decay time $\tau = 1.3$ ms

Table 4. Load cases performed for carbon-fiber/epoxy thick plates ($a/h = 17.4$, $f_0 = 2906$ *Hz)*

Cases	Characteristics of explosives (TNT)			Loadings		FSI parameter and impulse		
	C (kg)	R (m)	$S.F$	P_0 (MPa)	τ (ms)	I_0 (Ns.m^{-2})	ψ	I_t (Ns. m^{-2})
1	0.005	2.36	0.029	2.3	0.024	55.9	4.2	17.02
2	0.04	5.52	0.036	1.939	0.051	98.2	8.7	16.99
3	1.97	23.61	0.059	1.632	0.192	313.5	33.1	16.97
4	24.68	57.26	0.087	1.55	0.450	696.9	77.5	16.98
5	196.11	116.57	0.120	1.514	0.901	1363.4	155.3	17.00
6	586.94	169.32	0.143	1.5	1.300	1949.5	224.1	16.98

where $f_0 = \omega_{11}/(2\pi)$ *is the fundamental natural frequency (mode 1,1) of the plate,* $S.F = \sqrt{C}/R$ *is the shock factor,* P_0 *is the peak pressure,* τ *is the decay time,* $I_0 = P_0\tau$ *is the applied impulse related to the incident wave,* $\psi = \rho_w c_w \tau/m_s$ *is the FSI coefficient associated to the decay time and areal mass of the plate,* $I_t = 2I_0\psi^{-\psi/(\psi-1)}$ *is the reduced transferred impulse due to the FSI effect given by* (Taylor 1941).

Four different results are compared using: (1) LS-DYNA/USA (DAA_1) with cavitation, (2) LS-DYNA/USA (DAA_1) without cavitation, (3) analytical (DAA_1) without cavitation, and (4) analytical (two-step) approach. To evaluate the results, the following dimensionless parameter for the peak central deflection is introduced:

$$\bar{W}_{max} = \frac{w_{max}}{w_{taylor}} = \frac{\rho_w c_w}{2P_0\tau} w_{max} \tag{30}$$

where $w_{taylor} = 2P_0\tau/(\rho_w c_w)$ is the maximum displacement given by (Taylor 1941) if cavitation is not accounted at all, that is, by assuming that water can support tension.

The nondimensionalized results are plotted in Fig. 10. The valid regions for analytical (two-step) approach and analytical (DAA_1) approach are highlighted by using the red and blue (dotted) boxes respectively. It can be seen that the analytical (DAA_1) approach works quite well for the region bounded by $\tau/T_0 \geq 2.1$ ($\psi \geq 33$) because the decay time of the loading is relatively long compared to the plate (in-air) response time in that region. Both of the LS-DYNA/USA (DAA_1) results (with/without cavitation) converge to that of the analytical ones and the discrepancy is found to be within $\pm 15\%$, see Fig. 10 (right). Also, it can be found that all the results of analytical (two-step) approach are underestimated in that region because the transferred impulse given by Taylor's formulation is no longer sufficient to capture the continuing action of the FSI.

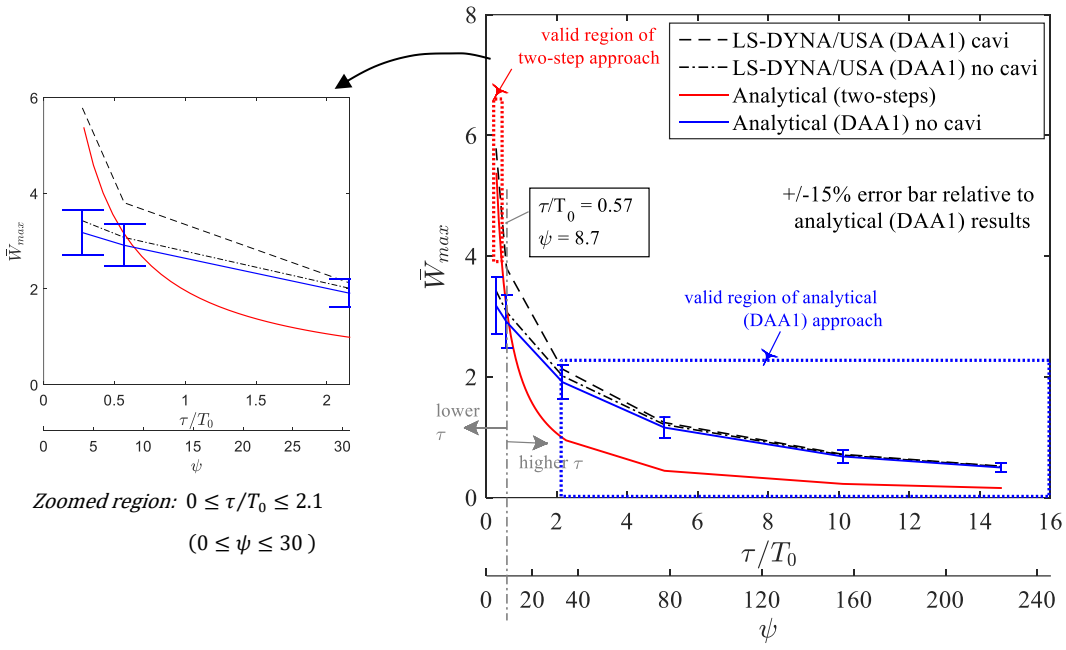

Fig. 10. Sensitivity to change of FSI parameter ψ on the response of thick CFRP plate ($a/h = 17.4$, $f_0 = 2906$ Hz)

The valid region for analytical (two-step) approach is directly taken from (Sone Oo et al. 2020). The zoomed plot on the left highlights the region where cavitation effect starts to become important.

On the other hand, the zone bounded by the red (dotted) box shows the valid region of the analytical (two-step) approach. This is the region where the cavitation effect is likely to be more significant. This is obvious by observing the two numerical results (with/without cavitation). The LS-DYNA/USA (DAA_1) with cavitation clearly shows larger dimensionless peak deflections than the numerical results without the cavitation effect, see the zoomed plot on the left of Fig. 10. In this case, the present analytical (DAA_1) approach underestimates the response since this model allows negative pressures, recall Fig. 5(b), which could later impose a nonphysical suction effect to the plate. According to Fig. 10, this suction effect seems to be much more significant for lower values of FSI parameter ψ or the time ratio, τ/T_0, leading to such underestimations by the analytical (DAA_1) approach without cavitation. Note that this conclusion is equally true for the LS-DYNA/USA (DAA_1) model without cavitation as well.

Another interesting observation is that the two-step approach seems to converge to the numerical model with cavitation notably before $\tau/T_0 < 0.57$ ($\psi < 8.7$). It means that the two-step model could correctly account for the pressure cut-off time and the associated energy provided that the decay time is relatively short. It should, nonetheless, be aware that the two-step approach could later lead to overestimation of the results if shorter decay times are considered (Sone Oo *et al.* 2020). The action regarding the cavitation could possibly make the analysis not only more complex but also nonlinear. Indeed, more attentions need to be paid regarding the action of cavitation in the future.

6. Advantages and limitations

In this section, the advantages and limitations of the present analytical model are discussed. Some of the main advantages of the proposed analytical (DAA_1) model include:

- the closed-form like expressions that could be easily implemented in any programming tool,
- reasonable accuracy if applied in the valid region (with discrepancy $< \pm 15\%$ compared to numerical model involving DAA_1)
- the potential to include post-damage behavior since the current formulations can be readily extended to analyze stresses and strains, see Fig. 11 in which the in-plane stresses in the CFRP plate subjected to an exponential loading ($P_0 = 1.5$ MPa and $\tau = 1.3$ ms) are calculated and confronted against LS-DYNA/USA (DAA1) results as an example case study,

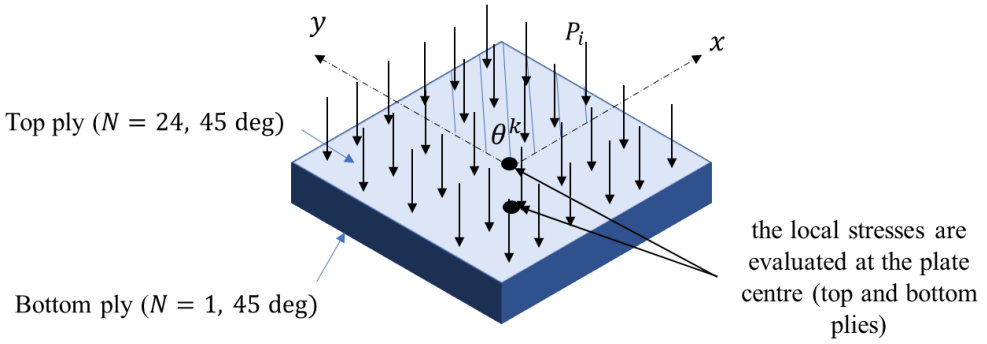

(a) Locations where in-plane (local) stresses are evaluated

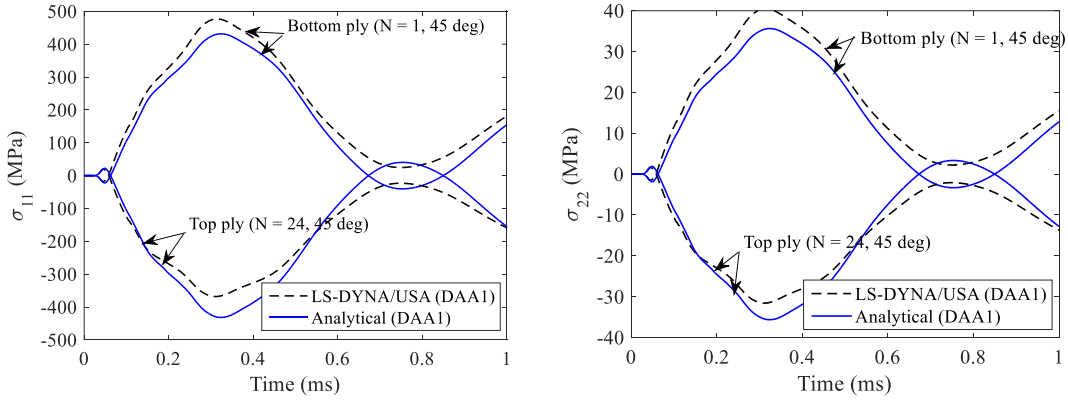

(b) Stresses in fiber direction (σ_{11}) Vs time

(c) Stresses in transverse direction (σ_{22}) Vs time

Fig. 11. Example case study for the analyses of in-plane stresses on CFRP thick plate ($a/h = 17.4$) subjected to exponential loading ($P_0 = 1.5$ MPa and $\tau = 1.3$ ms)

- saving of the computational time as shown in Table 5,
- some pre-processing stage such as meshing in numerical tool could be avoided, and finally
- such analytical tool is aimed to be applied at the pre-design stage to optimize the required design configuration when several different UNDEX scenarios need to be considered.

Note that the calculations shown in Table 5 are performed on the same computer (Core i7-8550U @1.8GHz, RAM 16 GB) and for the same termination time. The number of degrees of freedom (DOFs) involved is listed as well. As can be seen, the analytical (DAA_1) approach takes little or no time to complete the calculations while the numerical approach (LS-DYNA/USA) can be much more expensive depending on the number of DOFs involved. Therefore, the proposed analytical model may be used especially in the pre-design stages where different lamination schemes, different loadings as well as plate geometries need to be considered.

On the downside, it must be pointed out that the simplified analytical formulations are usually restricted to only one type of problem geometry. More derivations need to be done if a different geometry or boundary condition (e.g., clamped edges) is desired. The observations also suggest that the current analytical (DAA_1) model needs improvement in the action of cavitation, the geometric nonlinearity caused by large deflection, and the possible influence of the post-damage behavior.

Table 5. Comparison of the typical computation time between analytical (DAA_1), and LS-DYNA/USA (DAA_1) approaches

Cases	Termination time (ms)	Analytical (DAA_1)		LS-DYNA/USA (DAA_1)	
		DOF	Time (s)	DOF	Time (s)
Thin CFRP plate ($a = b = 400$ mm)	8	3	2.40	4681	208
Thick CFRP plate ($a = b = 100$ mm)	5	3	1.96	1345	96

7. Conclusions and perspectives

In this paper, the first-order Doubly Asymptotic Approximation is coupled to the analytical structural equations to predict the underwater blast response of spring-supported rigid plate and simply-supported deformable plates. Air-backed condition is considered for both cases. Structural damping, hydrostatic pressure as well as material damage effects are disregarded. Uniformly distributed dynamic step loading and plane shock exponential loadings are applied. Nonstandard finite difference (NSFD) scheme is used to derive the closed-form like analytical solutions. The obtained analytical (DAA_1) results are preliminarily tested on rigid plate as well as isotropic and orthotropic plates and are confronted against LS-DYNA/USA (DAA_1), and theoretical solutions based on Taylor's FSI theory. As for the rigid plate-spring system, the analytical (DAA_1) results agree excellently with those from LS-DYNA/USA (DAA_1) simulation with or without cavitation effect. The analytical solutions based on Taylor's theory either shows underestimation or non-physical long-time response due to the ignorance of water-added mass effect. As for the deformable model, oscillations are observed especially in the total pressure and acceleration results. After comparing the first four natural frequencies, the water-added mass formulation proposed by (Greenspon 1961) is modified to improve its accuracy especially regarding the higher order modes. However, such improvement is not rigorously justified and thus, needs more investigation in the future.

Parametric studies are also performed by varying the aspect ratios of the plate as well as the loading levels. To make effective evaluations, previous analytical results based on two-step impulse approach are included in addition to the LS-DYNA/USA (DAA_1) results with and without cavitation. According to the various case studies performed in this paper,

- the current analytical result with DAA_1 is linearly proportional to the applied peak pressure and valid only before the geometric nonlinear effect (due to large deflection) becomes significant, that is, before the peak central deflection exceeds half the thickness of the plate,
- flexible thin plates with large aspect ratio are prone to be more influenced by the geometric nonlinear effect (large deflection) as compared to thick plates with small aspect ratio,
- changing the decay time would change the FSI parameter ψ as well as the time ratio (τ/T_0) between the decay time of the loading and the plate fundamental period of oscillation, which in turn could lead to a change in the action of cavitation, and
- the current method is found to be valid for the regions where cavitation is not important, that is, for cases involving relatively long decay time compared to the plate response time.

Considering the various conclusions drawn above, several improvements to the current analytical formulae may be made in the future.

- First of all, the structural formulations based on the Navier solution approach are valid only for the simply-supported boundary condition. To solve other types of boundary conditions such as clamped edges, a different type of solution function or an approximate method (e.g., Ritz's method) must be considered (Reddy 2004).
- Secondly, the formulations can be extended to include the geometric nonlinear effects caused by moderate or large rotation (von Karman's sense).
- Thirdly, the effect of failure is not considered yet. It would also be interesting to further extend the current formulations that include post-damage behavior by using damage parameters.
- Fourthly, the effect of structural damping, the viscoelastic behavior as well as material strain rate should be studied.

On characterizing the incident load, a simple plane shock wave associated with a far-field underwater explosion is adapted. This is in fact a simplified assumption. In the future, a spherical wave as well as the possible contribution of the oscillating gas bubble should be examined. Also, at the arrival of the shock wave onto the plate, the scattered pressure is simply considered as a combination of the fully-reflected pressure and radiated pressure caused by the plate movement. In reality, for composites, some part of the incident pressures might have transmitted into the plate and the other part reflected. This effect should be investigated too. In addition, there are open questions about how to take into account the action of cavitation especially regarding the reloading. Finally, the phenomena concerning with hydrostatic pressure and water-backed condition should be explored. Either condition could modify the total pressure and thus, the criterion for cavitation. These are some of the research works that should be considered in the future.

Acknowledgements

This research work has been granted financially by DGA Naval Systems, France within the framework of the project SUCCESS. The authors would also like to express their gratitude to Calcul-Meca and Multiplast companies for their technical assistance. Last but not least, the authors would like to thank Marc E. Songolo from ICAM (Nantes, France) for his helpful advice during the development of the mathematical model.

Appendix A. Calculation of stiffness K_{mn}

The stiffness K_{mn} is calculated as:

$$K_{mn} = K_{11} + \frac{2K_{12}K_{23}K_{13} - K_{12}^2K_{33} - K_{13}^2K_{22}}{K_{22}K_{33} - K_{23}^2} \tag{A1}$$

The stiffness terms K_{ij} (where $i, j = 1, 2, 3$) are expressed as follows:

$$K_{11} = A_{44}\left(\frac{n\pi}{b}\right)^2 + A_{55}\left(\frac{m\pi}{a}\right)^2 \tag{A2}$$

$$K_{12} = A_{55}\left(\frac{m\pi}{a}\right) \tag{A3}$$

$$K_{13} = A_{44}\left(\frac{n\pi}{b}\right) \tag{A4}$$

$$K_{22} = D_{11}\left(\frac{m\pi}{a}\right)^2 + D_{66}\left(\frac{n\pi}{b}\right)^2 + A_{55} \tag{A5}$$

$$K_{23} = \frac{mn\pi^2}{ab}(D_{11} + D_{66}) \tag{A6}$$

$$K_{33} = D_{22}\left(\frac{n\pi}{b}\right)^2 + D_{66}\left(\frac{m\pi}{a}\right)^2 + A_{44} \tag{A7}$$

where D_{11}, D_{22}, D_{66} are bending stiffnesses and A_{44}, A_{55} are shear stiffnesses. Their corresponding formulations can be found in any classical composite textbooks, for example (Reddy 2004).

Appendix B. Sensitivity to numerical damping in LS-DYNA/USA (DAA_1)

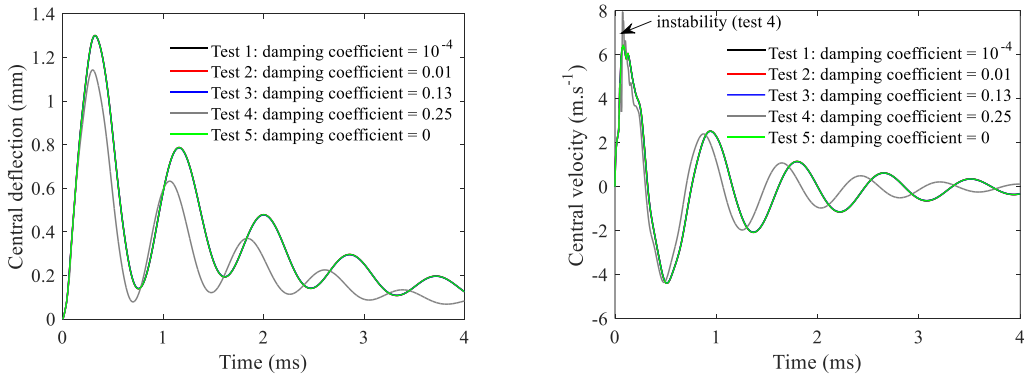

(a) Central deflection-time history *(b) Central velocity-time history*

Fig. B1. Sensitivity studies regarding numerical damping (Rayleigh stiffness damping coefficients) on LS-DYNA/USA (DAA_1) results (Tests performed on carbon fiber/epoxy plate using $P_0 = 1.5$ MPa and $\tau = 1.3$ ms)

Appendix C. Formulations for the analytical (two-step) approach

Stage I: calculation of maximum impulsive velocity

$$v_i = 2\frac{P_0\tau}{m_s}\,\psi^{-\psi/(\psi-1)} \tag{C1}$$

where $\psi = \rho_w c_w \tau/m_s$ is the FSI coefficient associated to impedance of water, decay time and areal mass of the plate (Taylor 1941). The associated time when maximum impulsive velocity is achieved can be predicted as $\tau_c = \tau\ln(\psi)/(\psi-1)$, which is also called cavitation inception time.

Stage II: determination of the free-response of the plate (including the water-inertia effect)

$$W_{mn} = 2A_{mn}v_i\frac{sin(\omega_{mn}t)}{\omega_{mn}} \tag{C2}$$

where $\omega_{\mathrm{mn}} = \sqrt{K_{mn}/\left(m_s + M_{f_{mn}}\right)}$ is the wetted natural frequencies for mode (m,n). The transverse deflection of the plate is given by using double Fourier series given in Eq. (17a), and the corresponding stiffness and water-added mass per unit area are already defined in Eqs. (A1) and (26) respectively.

More details about the derivations and the assumptions of the analytical (two-step) approach can be found in (Sone Oo *et al.* 2020).

References

Barras, G. 2012. "Interaction Fluide-Structure: Application aux Explosions Sous-Marines en Champ Proche." University of Sciences and Technologies, Lille, France.

Blevin, R.D. 1979. *Formulas for Natural Frequency and Mode Shape*. New York: Van Nostrand Reinhold Co.

Brochard, K., Le Sourne, H., and Barras, G. 2018. "Extension of the String-on-Foundation Method to Study the Shock Wave Response of an Immersed Cylinder." *International Journal of Impact Engineering* 117 (May 2017): 138–52. https://doi.org/10.1016/j.ijimpeng.2018.03.007.

Brochard, K., Le Sourne, H., and Barras, G. 2020. "Estimation of the Response of a Deeply Immersed Cylinder to the Shock Wave Generated by an Underwater Explosion." *Marine Structures* 72 (January).

Cole, R.H. 1948. *Underwater Explosions*. Princeton: Princeton University Press.

DeRuntz, J.A. Jr. 1989. "The Underwater Shock Analysis Code and Its Applications." In *Proceedings of the 60th Shock and Vibration Symposium*: 89–107.

Deshpande, V.S., Heaver, A., and Fleck, N.A. 2006. "An Underwater Shock Simulator." In *Proceedings of the Royal Society A*, Cambridge, UK, 1021–41.

Geers, T.L. 1978. "Doubly Asymptotic Approximations for Transient Motions of Submerged Structures." *The Journal of the Acoustical Society of America* 64: 1500–1508.

Greenspon, J.E. 1961. "Vibrations of Cross-Stiffened and Sandwich Plates with Application to Underwater Sound Radiators." *The Journal of the Acoustical Society of America* 33(11): 1485–97.

Hoo Fatt, M. S., & Sirivolu, D. 2017. Marine composite sandwich plates under air and water blasts. *Marine Structures*, *56*, 163–185. https://doi.org/10.1016/j.marstruc.2017.08.004

Hutchinson, J.W., and Xue, Z. 2005. "Metal Sandwich Plates Optimized for Pressure Impulses." *International Journal of Mechanical Sciences* 47(4-5 SPEC. ISS.): 545–69.

Kennard, E.H. 1943. "Cavitation in an Elastic Liquid." *Physical Review* 63(5 and 6): 172–81.

LSTC. 2017a. *LS-DYNA Keyword User's Manual, Volume I*. California, US.: Livermore Software Technology Corporation (LSTC). www.lstc.com.

LSTC. 2017b. *USA LS-DYNA User's Manual* (USA Release). California, US.: Livermore Software Technology Corporation (LSTC).

Mickens, R.E. 1993. *Nonstandard Finite Difference Models of Differential Equations*. World scientific. https://www.worldscientific.com/doi/abs/10.1142/2081.

Reddy, J.N. 2004. *Mechanics of Laminated Composite Plates and Shells*. 2nd ed. Florida: CRC Press LLC.

Schiffer, A., and Tagarielli, V. L. 2015. "The Response of Circular Composite Plates to Underwater Blast: Experiments and Modelling." *Journal of Fluids and Structures* 52: 130–44. http://dx.doi.org/10.1016/j.jfluidstructs.2014.10.009.

Schiffer, A., Tagarielli, V.L., Petrinic, N., and Cocks, A. 2012. "The Response of Rigid Plates to Deep Water Blast : Analytical Models and Finite Element Predictions." *Journal of Applied Mechanics* 79.

Sone Oo, Y. P., Le Sourne, H., and Dorival, O. 2020. "On the Applicability of Taylor ' s Theory to the Underwater Blast Response of Composite Plates." *International Journal of Impact Engineering* 145(July): 1–15. https://doi.org/10.1016/j.ijimpeng.2020.103677.

Sone Oo, Y. P., Le Sourne, H., and Dorival, O. 2019. “Development of Analytical Formulae to Determine the Response of Submerged Composite Plates Subjected to Underwater Explosion.” In *The 14th International Symposium on Practical Design of Ships and Other Floating Structures - PRADS 2019*, Yokohama, Japan, 1–21.

Songolo, M.E., and Bidégaray-Fesquet B. 2018. “Nonstandard Finite-Difference Schemes for the Two-Level Bloch Model.” *International Journal of Modeling, Simulation, and Scientific Computing* 9(4): 1–23.

Taylor, G.I. 1941. “The Pressure and Impulse of Submarine Explosion Waves on Plates.” In *The Scientific Papers of G. I. Taylor, Vol. III*, Cambridge, UK: Cambridge University Press, 287–303.